Supplementary Information: Anisotropic quantum emitter interactions in two-dimensional photonic-crystal baths.

Alejandro González-Tudela*,† and Fernando Galve*,¶

†*Instituto de Física Fundamental IFF-CSIC, Calle Serrano 113b, Madrid 28006, Spain.*

‡*Max-Planck-Institut für Quantenoptik Hans-Kopfermann-Str. 1. 85748 Garching, Germany.*

¶*I3M (UPV-CSIC) Institute for Instrumentation in Molecular Imaging, Universidad Politécnica de Valencia, 46022, Spain*

E-mail: a.gonzalez.tudela@csic.es; fernando.galve@i3m.upv.es

In this Supplementary Material, we provide more details on: i) Asymptotic expansions of the single QE self-energy; ii) Analytical continuation of the single quantum emitter (QE) self-energy to perform the exact integration of the excited state dynamics, $C_e(t)$; iii) Asymptotic scaling of the spatial decay of the extra bound state appearing in the middle band-gap; iv) Calculation of the fidelity of the four-qubit entangling protocol; v) the path to find the desired band-structure configuration in photonic-crystal implementations.

SM1 Self-energy expansions and analytical approximation of middle bound state energies.

The analytical formula for the self-energy for a QE coupled to the A sublattice reads:

$$\Sigma_e(z) = \frac{2g^2(z+\delta)}{\pi(z^2-\delta^2)}\mathrm{K}\left[\frac{16J^2}{z^2-\delta^2}\right]. \tag{SM1}$$

From here, it can be shown that around the middle band-edges:

$$\Sigma_e(\delta + x + i0^+) \approx \frac{g^2}{\sqrt{8}}\sqrt{\frac{\delta}{x}}\left[1+\frac{i}{\pi}\log\left(\frac{\delta x}{128J^2}\right)\right], \tag{SM2}$$

$$\Sigma_e(-\delta - x + i0^+) \approx \frac{g^2}{\sqrt{32}}\sqrt{\frac{x}{\delta}}\left[-1+\frac{i}{\pi}\log\left(\frac{\delta x}{128J^2}\right)\right]. \tag{SM3}$$

for $0 < x \ll J$. Thus, one middle band edge diverges as $1/\sqrt{x}$, as in 1D reservoirs, while the other one goes to zero as $\sqrt{x}$ as is the case in isotropic 3D reservoirs.

We can use these expansions, for example, to obtain an analytical approximation to the existence conditions of the middle-bound state (MBS), which is the main focus of the manuscript. On the lower band-edge $\Sigma_e(-\delta) = 0$, such that the critical detuning where the MBS disappears in the lower band-edge is just $\Delta_c = -\delta$. On the other band-edge, we can expand the self-energy for energies below the gap, finding:

$$\Sigma_e(\delta - x + i0^+) \approx -\frac{g^2}{\sqrt{8}\pi J}\sqrt{\frac{\delta}{x}}\log\left(\frac{128J^2}{\delta x}\right), \tag{SM4}$$

for $x \ll J$. Using this expansion, we can solve the pole equation analytically to obtain the energy of the MBS when $\Delta = \delta$, yielding to:

$$E_{\mathrm{MBS}} = \delta - \sqrt[3]{\frac{g^4\delta}{2(3\pi)^2J^3}\left(W\left(\frac{6144\pi J^4}{g^2\delta^2}\right)\right)^2}, \tag{SM5}$$

which agrees very well with the results of numerically solving the pole equation, as shown in

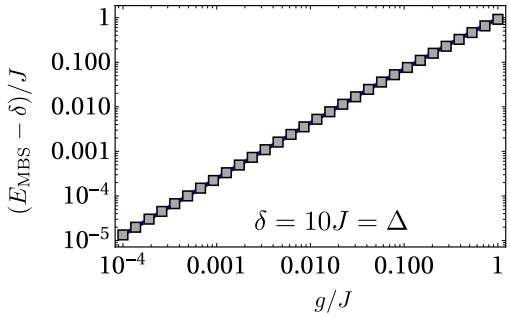

Figure SM1: (a) E_{MBS} as a function of g/J for a QE coupled to the A sublattice with $\Delta = \delta = 10J$. In markers the numerical results obtained by solving the exact pole equation, while in solid line the analytical result of Eq. SM5 obtained by expanding the solution of the self-energy close to the upper middle edge.

Fig. SM1.

SM2 Analytical continuation of the single QE self-energy

To fully characterize the different dynamical regimes one must integrate Eq. 6 of the main text exactly. To do the exact integration, we transform the integral above the real axis into a complex one by closing the contour of integration to apply Residue Theorem. Since the self-energy $\Sigma_e(z)$ is not analytical in certain regions, one can not simply close the contour with a semiarc in the lower half-plane. One possible choice of the detours to avoid the non-analytical regions is to take $E_{\mathrm{BC}} \pm 0^{\pm} - iy$ for four values of $E_{\mathrm{BC}} = -\sqrt{16J^2+\delta^2}, -\delta, \delta, \sqrt{16J^2+\delta^2}$. This divides the lower complex plane in five regions, where the definition of $\Sigma_e(z)$ must be adapted. To guarantee that we go to the correct Riemann surface of $\Sigma_e(z)$:

- In regions I, III, and V, defined by $\mathrm{Re}(z) \in (-\infty, -\sqrt{16J^2+\delta^2})$, $(-\delta, \delta)$ and $(\sqrt{16J^2+\delta^2}, \infty)$, respectively, one must use the definition of $\Sigma_e(z)$ as written in Eq. 7 of the main text.

- In regions II and IV, defined by $\mathrm{Re}(z) \in (-\sqrt{16J^2+\delta^2}, -\delta)$, and $(\delta, \sqrt{16J^2+\delta^2})$, one must adapt the definition of the self-energy as follows:

$$\Sigma_e(z) = \frac{2g^2(z+\delta)}{\pi^2(z^2-\delta^2)}\left(\mathrm{K}\left[\frac{16J^2}{z^2-\delta^2}\right] \pm 2i\mathrm{K}\left[1-\frac{16J^2}{z^2-\delta^2}\right]\right), \tag{SM6}$$

With these changes in the definition, one can now perform the exact integration of the dynamics separating the different contributions, as we did in Fig. 2 of the main text.

SM3 Asymptotic scaling of the BS wavefunction

The bound state wavefunction of a single QE in the single excitation subspace for our type of bath generally has the form:

$$|\Psi\rangle_{\rm BS} = \left[C_e \sigma_{eg} + \sum_{\mathbf{k}} \left(C_a(\mathbf{k}) a^\dagger_{\mathbf{k}} + C_b(\mathbf{k}) b^\dagger_{\mathbf{k}} \right) \right] |{\rm vac}\rangle \,, \tag{SM7}$$

where $|{\rm vac}\rangle$ is the global vacuum of the combined QE-bath system. By solving $H|\Psi\rangle_{\rm BS} = E_{\rm BS}|\Psi\rangle_{\rm BS}$, one arrives to:

$$C_A(\mathbf{k}) \propto \frac{E_{\rm BS} + \cos(2\theta_{\mathbf{k}})\omega(\mathbf{k})}{E_{\rm BS}^2 - \omega(\mathbf{k})^2} e^{-i\mathbf{k}\mathbf{n}_e} \,, \tag{SM8}$$

$$C_B(\mathbf{k}) \propto -\frac{\omega(\mathbf{k})\sin(2\theta_{\mathbf{k}})}{E_{\rm BS}^2 - \omega(\mathbf{k})^2} e^{-i(\mathbf{k}\mathbf{n}_e + \phi(\mathbf{k}))} \,., \tag{SM9}$$

for a QE coupled to the A lattice site at position $\mathbf{n}_e$. To make a more quantitative estimation of the decay of the wavefunction, we can consider that the larger contribution to the integrand of $C_{A/B}(\mathbf{k})$ will come from the points closer to the band edge, $\omega(\mathbf{k}) \approx \delta$. At these points $\cos(\theta_{\mathbf{k}}) \approx 1$, $\sin(\theta_{\mathbf{k}}) \approx 0$, and the energy dispersion is expanded, e.g.,

$$\omega(\pi - q_1, \pi - q_2) \approx \delta \left(1 + \frac{q_1^2 q_2^2}{2\delta^2} \right) , \tag{SM10}$$

for $q_{1,2} \ll 1$. Focusing on $C_A(\mathbf{n})$, the sum of the contribution around the band-edge frequencies can be rewritten:

$$C_A(\mathbf{n}) \approx \frac{2}{(2\pi)^2\delta}\left[(-1)^{(n_1+n_2)}\iint_0^{2\pi} d^2\mathbf{q}\frac{\mathrm{Re}\left[e^{i(q_1n_1+q_2n_2)}\right]}{1+\frac{q_1^2q_2^2}{2\delta^2}}+\right.$$
$$\left.(-1)^{(n_1-n_2)}\iint_0^{2\pi} d^2\mathbf{q}\frac{\mathrm{Re}\left[e^{i(q_1n_1-q_2n_2)}\right]}{1+\frac{q_1^2q_2^2}{2\delta^2}}\right]. \tag{SM11}$$

To continue the derivation, let us restrict to a particular direction, e.g., $n_1 \equiv n$ and $n_2 = 0$. Notice, that since we have made the expansion for $q_i \ll 1$, the upper limit of the integral should not matter since the main contribution will be coming from $q_i \to 0$. Then, we can in principle extend the integral to infinite. Using this, and the fact that:

$$\int_0^\infty dq_1 \frac{\cos(q_1 n)}{1+\frac{q_1^2q_2^2}{2\delta^2}} = \frac{e^{-\sqrt{2}n\delta/q_2}\pi\delta}{\sqrt{2}q_2}, \tag{SM12}$$

we arrive to:

$$C_A(n,0) \approx \frac{(-1)^n}{\pi\sqrt{2}}\left[\int_0^\infty dq_2 \frac{e^{-\sqrt{2}n\delta/q_2}}{q_2}\right]. \tag{SM13}$$

The problem of the previous integral is that it does not converge because the integrand scales as $1/q_2$ when $q_2 \to \infty$. However, we know there should be a natural cut-off given by discretization. Thus, we replace ∞ by q_c and find that:

$$C_A(n,0) \approx \frac{(-1)^n}{\pi\sqrt{2}}\Gamma(0,\sqrt{2}n\delta/q_c). \tag{SM14}$$

where $\Gamma(a,z)$ being the incomplete Γ-function. We can use the analytical expansions of the Γ to

obtain the approximated analytical scaling in the small/large band-gap limit, that is:

$$\Gamma(0, x \ll 1) \approx -\gamma + \log(1/x)\,, \tag{SM15}$$

$$\Gamma(0, x \gg 1) \approx \frac{e^{-x}}{x}\,, \tag{SM16}$$

where $\gamma \approx 0.577$ is the Euler constant. Thus, the wavefunction shows a very slow logarithmic decay when $\sqrt{2}n\delta/q_c \ll 1$, while having a Yukawa-type decay when $\sqrt{2}n\delta/q_c \gg 1$.

SM4 Four-qubit entangling protocol

Let us study in detail how the entangling protocol works in the simplest configuration, that is, when all the Raman lasers act equally in all the atoms and without considering other decoherence sources. We assume that all the atoms are initially in the ground state, $|\Psi_0\rangle = |g\rangle_a \otimes |g\rangle^{\otimes 4}$, while the bath is also in the vacuum state. Next, with a microwave field we switch the auxiliary atom to the e state with a π-pulse, such that $|\Psi_1\rangle = |e\rangle_a \otimes |g\rangle^{\otimes 4}$. Then, we switch on all the Raman lasers, Ω, such that the QEs can interact between themselves by exchanging/absorbing bath excitation with the assistance of the Raman laser. Since, we start effectively with a single excitation in the five QEs, the effective dynamics can be written in a subspace: $B = \{|e\rangle_a \otimes |g\rangle^{\otimes 4}, |g\rangle_a \otimes \sigma^i_{eg} |g\rangle^{\otimes 4}\}$, with $i = 1,2,3,4$. In this basis, the effective Hamiltonian governing the interaction:

$$H_{\text{eff}} = \begin{pmatrix} \Delta & J_a & J_a & J_a & J_a \\ J_a & \Delta & J_1 & J_2 & J_1 \\ J_a & J_1 & \Delta & J_1 & J_2 \\ J_a & J_2 & J_1 & \Delta & J_1 \\ J_a & J_1 & J_2 & J_1 & \Delta \end{pmatrix} \tag{SM17}$$

It is instructive to rewrite this effective Hamiltonian in a basis, $B' = \{|\alpha_i\rangle\}_{i=1}^5$, that contains the state we want to obtain, that is: $|\Psi\rangle_{\text{goal}} = |g\rangle_a \otimes \frac{1}{2}\sum_i \sigma^i_{eg} |g\rangle^{\otimes 4}$. This is achieved with the following

unitary transformation:

$$U = \begin{pmatrix} 1 & 0 & 0 & 0 & 0 \\ 0 & \frac{1}{2} & \frac{1}{2} & \frac{1}{2} & \frac{1}{2} \\ 0 & \frac{1}{2} & \frac{1}{2} & -\frac{1}{2} & -\frac{1}{2} \\ 0 & \frac{1}{\sqrt{2}} & -\frac{1}{\sqrt{2}} & 0 & 0 \\ 0 & 0 & 0 & \frac{1}{\sqrt{2}} & -\frac{1}{\sqrt{2}} \end{pmatrix} \tag{SM18}$$

where $|\alpha_1\rangle = |\Psi_1\rangle$ and $|\alpha_2\rangle = |\Psi\rangle_{\text{goal}}$. In this new basis, the effective Hamiltonian reads:

$$H_{\text{eff}} = \Delta\mathbf{1} + \begin{pmatrix} 0 & 2J_a & 0 & 0 & 0 \\ 2J_a & 2J_1+J_2 & 0 & 0 & 0 \\ 0 & 0 & -J_2 & 0 & 0 \\ 0 & 0 & 0 & -J_1 & J_2-J_1 \\ 0 & 0 & 0 & J_2-J_1 & -J_1 \end{pmatrix}. \tag{SM19}$$

One immediately realizes that our initial state is indeed only coupled to the desired state, $|\Psi\rangle_{\text{goal}}$, due to the spatial symmetry of our initial state. Then, the fidelity of the protocol can be obtained by solving the dynamics in the restricted 2×2 subspace, yielding:

$$F = |\left\langle \Psi_{\text{goal}} \right| e^{-iH_{\text{eff}}t} |\Psi_1\rangle|^2 = \frac{16J_a^2}{R^2}\sin^2(Rt/2), \tag{SM20}$$

with $R = \sqrt{(2J_1+J_2)^2+16J_a^2}$. Thus, choosing the time duration of the operation $RT = \pi$, we maximize the excitation transfer and the fidelity, yielding:

$$F_{\text{max}} = |\left\langle \Psi_{\text{goal}} \right| e^{-iH_{\text{eff}}t} |\Psi_1\rangle|^2 = \frac{16J_a^2}{(2J_1+J_2)^2+16J_a^2}. \tag{SM21}$$

SM5 Photonic crystal implementation

The quest for a photonic crystal structure which can mediate such directional interactions requires two ingredients: (i) two bands separated by a photonic band-gap, (ii) with (at least one of the) band-edges with the square-like shape in momentum space required to obtain the directional character. While (ii) appears pretty naturally in square geometries with a dimer-like structure, the combination of (i-ii) seems not to be so straightforward. In Fig. SM2, we plot the dielectric structure and the projected band-diagrams of several structures we analyzed before arriving to the one shown in figure 7 of the main manuscript:

- In Figs. SM2(a-b), we start considering one of the simplest dimerized geometries deforming a simple square lattice geometry in a GaAs slab ($\varepsilon_r = 13$) by making the holes of different sizes. We see that even though independently the bands satisfy the (ii) condition, there is no band-gap between two bands, irrespective of the size of the holes. Similar configurations (not shown) with different hole geometries did not give provide any clear advantage either.

- Another way of dimerizing the simple square geometry is by filling one of two holes by another material. In Fig. SM2(c) we show the case of a diamond slab ($\varepsilon_r = 6$) and GaAs 'holes' in addition to normal air holes. We observe that this approach allows to open the gap, even though a very small one.

- Finally, in Fig. SM2(d) we show how by combining both approaches: different hole sizes and different materials, one can open a more robust band-gap with the desired behaviour, as we explain in the main manuscript.

Though this provides a path on how to design structures with the desired band-structure behaviour, we acknowledge it may not be the only one. Further optimization procedures, e.g., based on inverse design methods [1,2], might provide alternative and better paths.

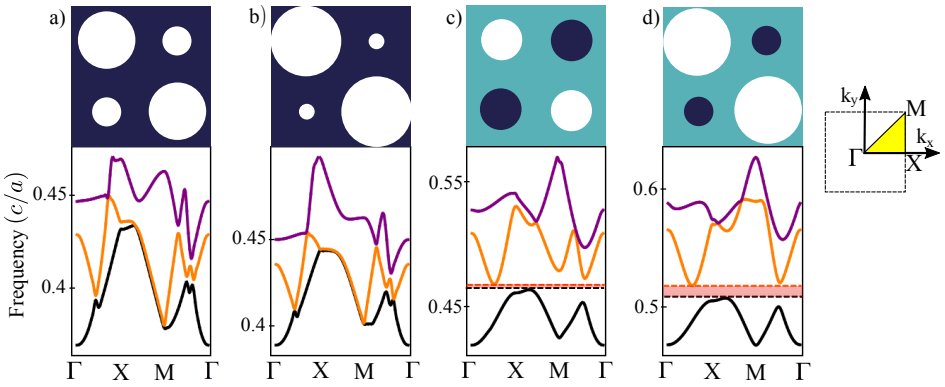

Figure SM2: Sequential quest for a gapped dispersion. In the top/bottom panel, we plot the dielectric structure/corresponding projected band-diagram. Configurations with only one dielectric material (a,b) were not found to give a workable gap, irrespective of the size and relative position of holes in a slab. A second dielectric material was required to open the gap (c), which gives the optimal solution (d) in the main article. The parameters are a) GaAs ($\varepsilon_r = 13$) slab with $r_1 = 0.1a$, $r_2 = 0.2a$ air holes, b)GaAs slab with $r_1 = 0.05a$, $r_2 = 0.25a$ air holes, c) Diamond ($\varepsilon_r = 6$) slab with $r_1 = 0.2a$ (GaAs) and $r_2 = 0.2a$ (air) holes, d) Diamond slab with $r_1 = 0.15a$ (GaAs) and $r_2 = 0.35a$ (air) holes. The three bands are for z-odd modes in the 3rd (black), 4th (orange) and 5th (purple) bands.

References

(1) Sapra, N. V.; Vercruysse, D.; Su, L.; Yang, K. Y.; Skarda, J.; Piggott, A. Y.; Vučković, J. Inverse design and demonstration of broadband grating couplers. *arXiv:1808.07630* **2018**,

(2) Molesky, S.; Lin, Z.; Piggott, A. Y.; Jin, W.; Vucković, J.; Rodriguez, A. W. Inverse design in nanophotonics. *Nature Photonics* **2018**, *12*, 659.